Microchimica Acta
https://doi.org/10.1007/s00604-019-3372-2

ORIGINAL PAPER

A voltammetric biosensor for mercury(II) using reduced graphene oxide@gold nanorods and thymine-Hg(II)-thymine interaction

Huali Jin[1] · Mingli Zhang[1] · Min Wei[1] · Jun-Hu Cheng[2]

Received: 29 November 2018 / Accepted: 20 March 2019

Abstract

The presented voltammetric mercury(II) sensor is based on the specific interaction between Hg(II) ion and thymine-thymine base pairs. Reduced graphene oxide is functionalized with gold nanorods and then loaded with thionine and streptavidin (RGO@AuNR-TH-SA). A T-rich thiolated DNA (S1) is firstly immobilized on a gold electrode. In the presence of Hg (II), the T-rich biotin-DNA (biotin-S2) binds to S1 via T-Hg(II)-T interaction. Then, the RGO@AuNR-TH-SA is linked to the gold electrode by specific binding between SA and biotin-S2. This produces an electrochemical signal (at −0.208 V vs. Ag/AgCl) of TH that depends on the concentration of Hg (II). The peak current increases linearly in the 1 to 200 nM Hg (II) concentration range, and the detection limit is 0.24 nM. The sensor is highly selective for Hg (II) over other environmentally relevant metal ions, even at concentration ratios of >1000.

Keywords Thionine · Streptavidin-biotin · Differential pulse voltammetry · Signal amplification

Introduction

The sensitive and selective detection of mercury ion (Hg^{2+}) is crucial to food safety and environmental protection [1]. Various methods such as fluorimetry, colorimetry, atomic absorption/emission spectroscopy, inductively coupled plasma mass spectrometry, and surface-enhanced Raman scattering have been successfully developed to detect Hg^{2+} [2–4]. Among these methods, electrochemical techniques have received comprehensive attention on account of its simple operation, low cost and easiness for miniaturization [5]. Since the specific reciprocity between Hg^{2+} and thymine (T)-thymine (T) was studied [6], multifarious DNA-based electrochemical biosensors for Hg^{2+} detection have been established [7, 8]. To fabricate the favorable electrochemical biosensor, the load of biomolecules and electrochemical probe is very momentous.

Reduced graphene oxide (RGO) has been extensively used in electrochemical biosensors on account of its sufficient surface area and excellent electronic transmission ability [9]. On the other hand, RGO can be used as carrier for immobilizing single-stranded DNA by hydrophobic and π-stacking interactions. So the popular detection principle is based on the combination or dissociation of DNA from the RGO surface [10]. However, this may result in the complicated circumstances and the experimental instability. It has been reported that RGO can act as a nanoscaffold for aromatic compounds via π-interaction and/or Vander Waals' force [11]. As a result of its planar aromatic structure, thionine (TH), as a kind of electroactive probe, can be effectively adsorbed onto RGO by mighty π-stacking interactions and non-covalent charge transfer to realize the signal amplification strategy [12]. On the other hand, due to their outstanding conductivity and good stability, gold nanorods (AuNRs) have been extensively applied to electrochemical sensors as a carrier for amplifying signals [13–15]. AuNRs can be used to load more streptavidin (SA) and TH by Au-NH_2 bond as a secondary signal

Electronic supplementary material The online version of this article (https://doi.org/10.1007/s00604-019-3372-2) contains supplementary material, which is available to authorized users.

✉ Min Wei
wei_min80@163.com

✉ Jun-Hu Cheng
chengjunhu1229@163.com

[1] College of Food Science and Technology, Henan Key Laboratory of Cereal and Oil Food Safety Inspection and Control, Henan University of Technology, Zhengzhou 450001, People's Republic of China

[2] School of Food Science and Engineering, South China University of Technology, Guangzhou 510641, People's Republic of China

Published online: 30 March 2019

amplification strategy. As far as we know, there are few reports on the electrochemical detection of Hg^{2+} using RGO@AuNR as the carrier to load SA and TH (RGO@AuNR-TH-SA).

A novel electrochemical T-Hg^{2+}-T biosensor based on RGO@AuNR-TH-SA was firstly developed to detect Hg^{2+}. Figure 1 shows that the T-rich thiolated DNA (S1) was fixed at the gold electrode (AuE). In the absence of Hg^{2+}, the T-rich biotin-DNA (biotin-S2) cannot be attached to the surface of the AuE. Hence, the GR@AuNR-TH-SA cannot bind to the AuE surface. This results in a smaller electrochemical signal of TH due to lower physical adsorption. In the presence of Hg^{2+}, Hg^{2+} can interact with T-T pairs between S1 with biotin-S2 and form stable T-Hg^{2+}-T structures on the AuE surface. Then, RGO@AuNR-TH-SA was connected to the AuE by specific binding of SA and biotin, giving rise to the enhancement of electrochemical signal of TH.

Experimental

Materials and reagents

The S1 and biotin-S2 were purchased from Sangon biotech Co. Ltd. (Shanghai, China. https://www.sangon.com/). Their sequences used are as follows: S1:5′-SH-TTT TTT T-3′. Biotin-S2: 5′-biotin-TTT TTT T-3′. Reduced graphene oxide (RGO) flakes with the thickness of 0.55–3.74 nm were obtained from TIME NANO (Chengdu, China. http://www.timesnano.com). The Categories No of product is TNRGO. $HgCl_2$, thionine (TH) and 5-Bromosalicylic acid were bought from Shanghai yuanye Bio-Technology Co., Ltd. (Shanghai, China. http://www.shyuanye.com/). Chitosan and streptavidin (SA) were both purchased from Solarbio Science and Technology Co., Ltd. (Beijing, China. http://solarbio.bioon.com.cn/). 6-mercapto-1-hexanol (MCH) were purchased from Aladdin (http://www.aladdin-e.com/us_en/) and was used to block the nonspecific binding sites on the electrode surface. The other reagents were of analytical grade. Tris-HCl buffer solutions (Tris-HCl) were prepared by using 50 mM Tris, 0.2 M NaCl and 1.0 mM EDTA. The ultrapure water was used throughout the experiments.

Apparatus

Electrochemical experiments were accomplished on CHI-660E electrochemical workstation (Chenhua Instrument Co., Shanghai, China). The three electrode system consists of that AuE, Ag/AgCl and platinum wire used as working electrode, reference electrode and auxiliary electrode, respectively.Electrochemical Impedance Spectroscopy (EIS) was performed in 10 mM $[Fe(CN)_6]^{3-/4-}$ solution containing 0.1 M KCl, at a signal amplitude of 5 mV in the frequency range of 100 kHz to 100 mHz. Differential Pulse Voltammetry (DPV) was recorded in the potential range from −0.5 to 0 V vs Ag/AgCl in a 50 mM Tris-HCl solution. The parameters applied were the following: 0.05 V pulse amplitude, 0.05 s pulse width, and 0.5 s pulse period.

The elemental analysis were performed on an elemental analyzer (Thermo Fisher Flash 200). The

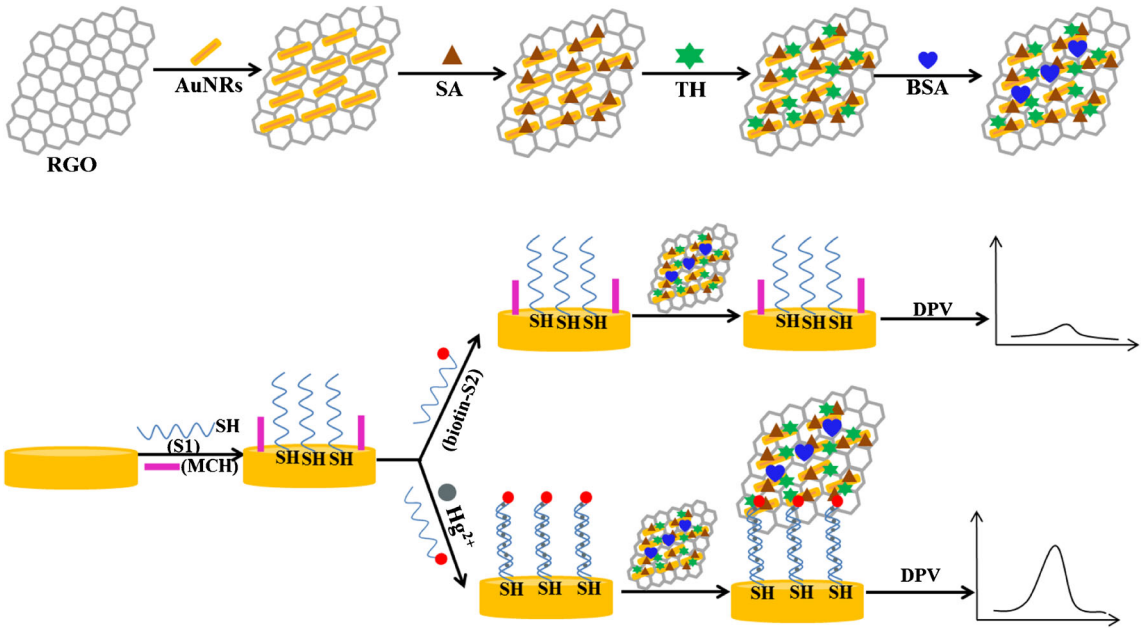

Fig. 1 Schematic illustration of the electrochemical Hg^{2+} biosensor

morphology of the prepared materials was characterized by Transmission electron microscopy (TEM, FEI Tecnai G2 F20 S-TWIN). Powder X-ray diffraction (XRD) analysis was recorded on a Bruker D8 Advance (Bruker AXS, Germany) with a Cu Ka radiation source.

Preparation of RGO@AuNR and RGO@AuNR-TH-SA nanocomposites

The RGO (0.1 mg mL^{-1}) was ultrasonicized for 1 h to achieve homogeneous dispersions. Then 2 mL AuNR colloid (v:v = 1:1) was added. The RGO@AuNR nanocomposites were obtained by magnetic stirring for two hours.

0.05 g of chitosan was added into 0.1 M acetic acid solution to dissolve, and diluted to a 10 mL volumetric flask to obtain 5 mg mL^{-1} chitosan solution. 1 mg SA (dry powder) was added into 1 mL of the above CS solution and then mixed with a vortex mixer to obtain the chitosan-SA mixture.

The RGO@AuNR-TH-SA nanocomposites were prepared in this way. First, 2 μL 1.0 mg mL^{-1} chitosan-SA was vortexed with 40 μL RGO@AuNR for 10 min. After incubated for 0.5 h, it was centrifuged at 12000 rpm with 9576 Xg for 20 min and then redispersed with 40 μL 50 mM Tris-HCl. Then 4 μL 10 mg mL^{-1} TH was added with a shaking table for 0.5 h. After centrifuged, it was redispersed with 40 μL 50 mM Tris-HCl. Afterwards, 3 μL 1% (*w*/w) bovine serum albumin was added to the aforesaid solution to block the unbound active site on AuNRs. After incubated for 40 min, the RGO@AuNR-TH-SA nanocomposites were centrifuged and then redispersed in 40 μL 50 mM Tris-HCl (pH 7.4).

Fabrication of electrochemical biosensor

First, 5 μL 5 μM S1 was added dropwise to the clean AuE, and incubated at 37 °C for 1 h to obtain S1/AuE. After washing the S1/AuE with Tris-HCl, 5 μL 0.1 mM MCH was added dropwise to the electrode to passivate the free interspaces between S1. After washing, the MCH-S1/AuE was incubated with 5 μL solution containing 5 μM biotin-S2 and different concentrations of Hg^{2+} at 37 °C to cause a interaction reaction between S1 and biotin-S2. The electrode was denoted as Hg^{2+}/biotin-S2/MCH-S1/AuE. After gentle washing, the electrodes were incubated with 5 μL RGO@AuNR-TH-SA signal probe for 1 h at 37 °C to obtain RGO@AuNR-TH-SA/Hg^{2+}/biotin-S2/MCH-S1/AuE. After that, it was thoroughly washed with Tris-HCl to remove the redundant probes, and then performed DPV detection.

Results and discussion

Characterization of RGO@AuNR nanocomposites

The contents of RGO were confirmed by the Elemental analysis, and the results are as follows: The content of C, H, O, N is respectively 85.30%, 1.98%, 0.78%, 1.45%, indicating the reduction of graphene oxide. Figure 2a shows the FT-IR spectra of RGO and RGO@AuNR. The spectrum of RGO presents several absorption peaks at 3427 cm^{-1} (O-H), 1572 cm^{-1} (C=C) and 1229 cm^{-1} (C-O) (epoxy) [16]. For the spectrum of RGO@AuNR, the peaks at 3308 cm^{-1}, 2923 cm^{-1}, 2850 cm^{-1} and 1636 cm^{-1} are respectively the characteristic vibration of O-H groups, the asymmetric and symmetric stretching vibrations of methylene groups, and the stretching vibration of C=C [17, 18].

The XRD pattern of RGO@AuNR is shown in Fig. 2b. The pattern diffraction at 38.3°, 44.5°, 64.7°, 77.7° and 81.9° correspond to the peaks of Au(111), (200), (220), (311), and (222), respectively [17]. The characteristic peak at around 26 ° is attributed to the C (002) plane of RGO.

TEM was used to characterize the morphology of the different materials. As shown in Fig. 2c, the RGO are the thin flakes. Figure 2d shows that synthesized AuNRs have an obvious rod like structure, and the length and the diameter of AuNRs are about 47 nm and 12 nm respectively. As shown in Fig. 2e, it can be found that some AuNRs are attached onto the surface of RGO to form RGO@AuNR. The increased indistinct and opacity of Fig. 2f indicate the successful immobilization of SA on the surface of RGO@AuNR.

Feasibility characterization and study of the Hg^{2+} biosensor

EIS is adopted to characterize the biosensor. As shown in Fig. 3a, compared with bare AuE (curve a), the resistance increases when S1 is immobilized on the electrode (curve b) on account of the electrostatic repulsion between the negatively charged S1 and $[Fe(CN)_6]^{3-/4-}$. The assembly of the MCH (curve c) also produces an increase in resistance. In the absence of Hg^{2+}, when MCH-S1/AuE is incubated with biotin-S2 (curve d), the resistance remains almost unchanged. And then the signal probe is assembled (curve e), the resistance also remains invariant. In the presence of Hg^{2+}, when MCH-S1/AuE is incubated with biotin-S2 (curve f), the resistance increases significantly due to the occurrence of T-Hg^{2+}-T interaction. After assembly of the signal probe (curve g), the resistance decreases because RGO@AuNR nanocomposites can promote electron transfer. These results reveal the successful assembly of the biosensor.

The DPV responses of different electrodes in 50 mM Tris-HCl buffer (pH 7.4) are studied. As shown in Fig. 3b, the oxidation peak current value is 1.246 μA in the absence of

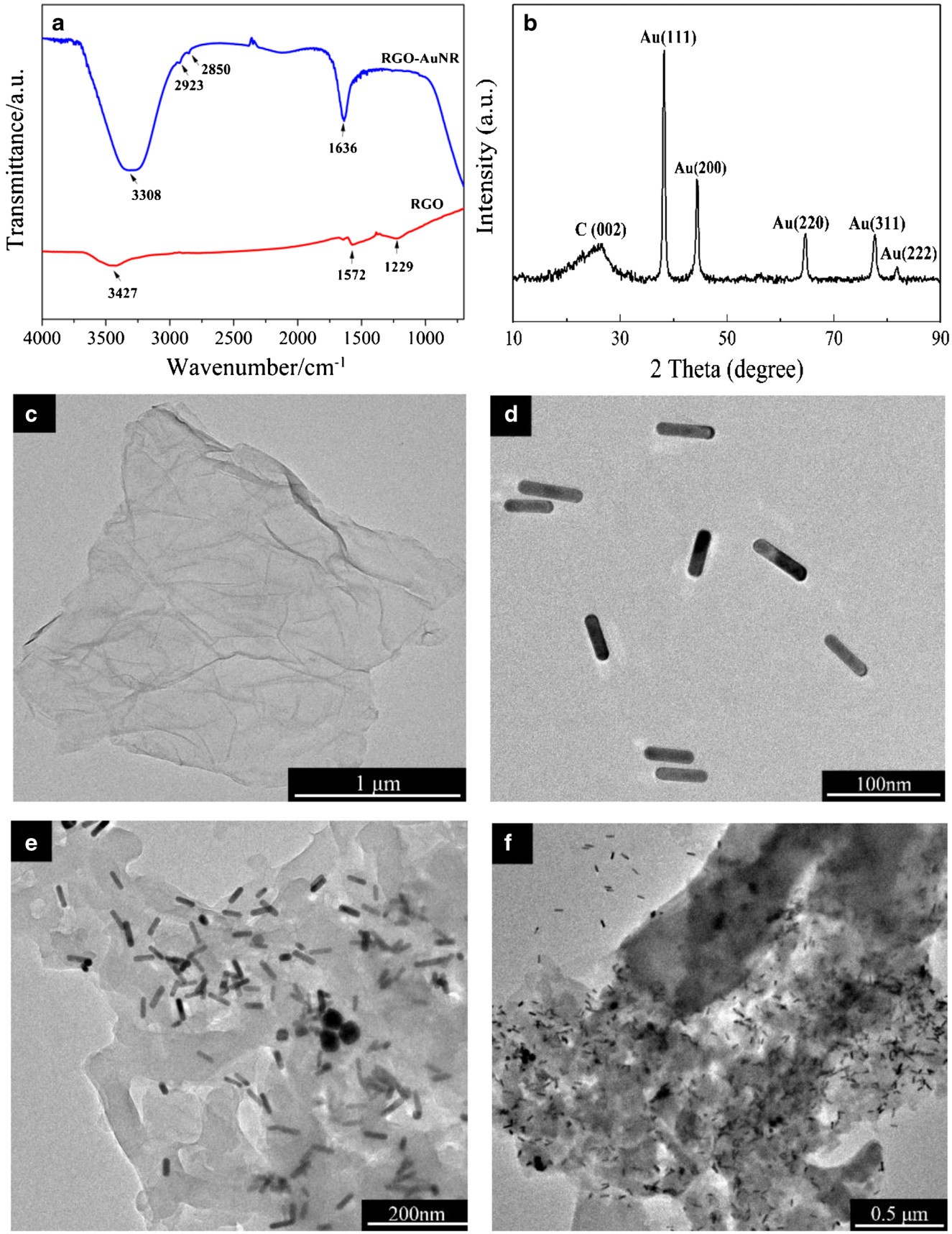

Fig. 2 **a** FTIR spectra of RGO and RGO@AuNR; **b** XRD pattern of RGO@AuNR; TEM images: **c** RGO; **d** AuNRs; **e** RGO@AuNR; **f** RGO@AuNR-SA

Hg^{2+} (curve a). In the presence of Hg^{2+} (curve b), it is 10.93 μA. The dramatical enhancement of peak current can be explained as follows: In the absence of Hg^{2+}, the biotin-S2 cannot interact with MCH-S1/AuE, so RGO@AuNR-TH-SA produces a smaller electrochemical signal by a little physical adsorption on the MCH-S1/AuE. In the presence of Hg^{2+}, biotin-S2 can successfully react with MCH-S1/AuE by the T-Hg^{2+}-T interaction, and RGO@AuNR-TH-SA can connect to the Hg^{2+}/biotin-S2/MCH-S1/AuE by specific binding of SA and biotin, bringing about the enhancement of electrochemical signal. The above results indicate that the biosensor is feasible for detecting Hg^{2+}.

Moreover, the DPV analysis is used to indicate the effect of the RGO@AuNR on the amplification of the electrochemical responses. As shown in Fig. 3c, the oxidation peak current of RGO@AuNR -TH-SA/Hg^{2+}/biotin-S2/MCH-S1/AuE is 10.81 μA (curve c), which is superior to that of RGO -TH-SA/Hg^{2+}/biotin-S2/MCH-S1/AuE (4.525 μA, curve b) and AuNR-TH-SA/Hg^{2+}/biotin -S2/MCH-S1/AuE (2.107 μA, curve a). As shown in Fig. 3d, the oxidation peak current of TH/AuNR/AuE (curve b) and TH/RGO/AuE (curve c) is respectively 7.369 μA and 10.69 μA, which is better than that of bare AuE (2.121 μA, curve a), but worse than that of TH/RGO@AuNR/AuE (28.1 μA, curve d). These results indicate that RGO@AuNR is a good choice for improving the biosensor performance due to the favorable adsorption to TH and SA.

Optimization of parameters

In order to improve the detection effects of the biosensor, the experimental parameters are optimized. Respective data and Figures are given in the Fig. S1. The following experimental conditions are found to give the best results: (a) Optimal concentration of TH: 10 mg mL^{-1}; (b) Optimal incubation time of S1: 60 min; (c) Optimal interaction time of S1 and biotin-S2: 2 h; (c) Optimal accumulation time: 60 min.

Sensitivity of the biosensor

Under the optimal experimental conditions, the biosensor is used for quantitative detection of Hg^{2+} by DPV. As

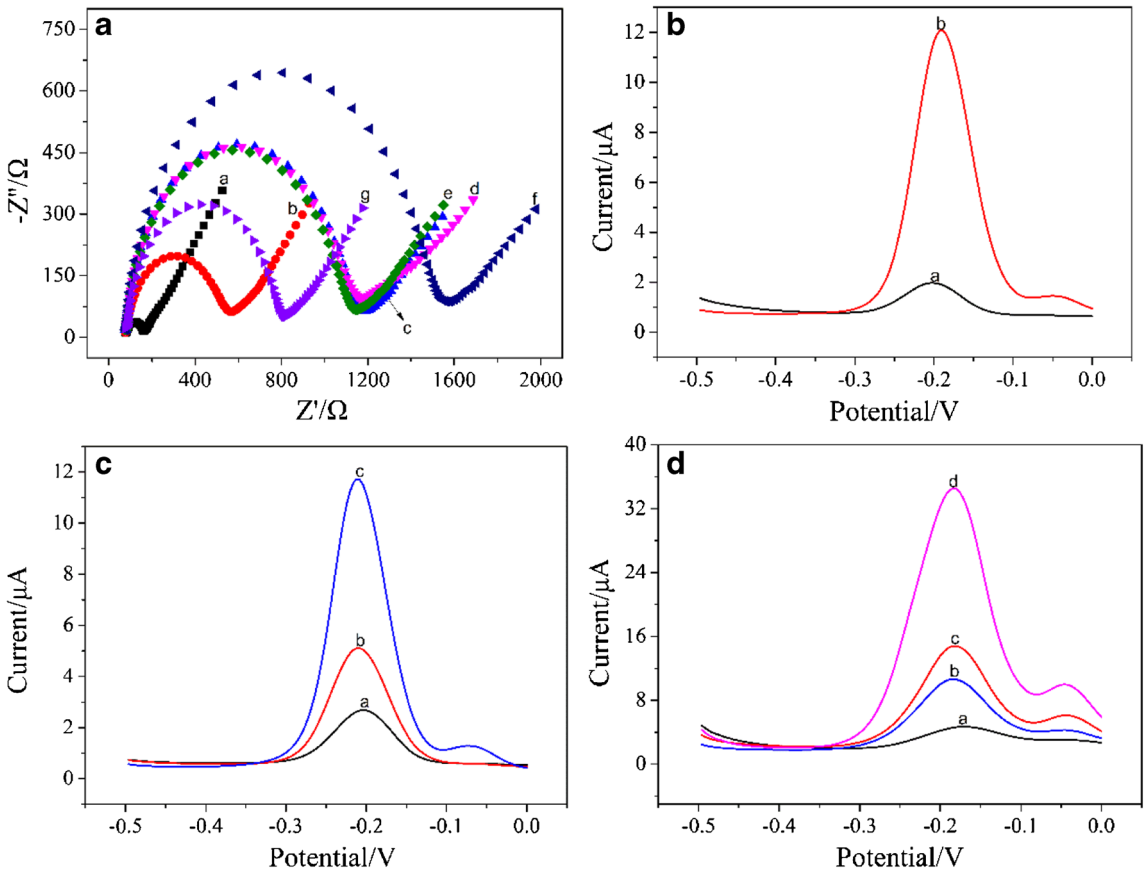

Fig. 3 **a** EIS of the bare AuE (a), S1/AuE (b), MCH-S1/AuE(c), biotin-S2/MCH-S1/AuE(d), RGO@AuNR-TH-SA/biotin-S2/MCH-S1/AuE(e), Hg^{2+}/biotin-S2/MCH-S1/AuE(f), and RGO@AuNR-TH-SA/Hg^{2+}/biotin-S2/MCH-S1/AuE (g); **b** DPV curves of the biosensor in the absence of Hg^{2+} (curve a) and in the presence of 100 nmol/L Hg^{2+} (curve b); **c** DPV curves of the AuNR-TH-SA/Hg^{2+}/biotin-S2/MCH-S1/AuE (a), RGO-TH-SA/Hg^{2+}/biotin-S2/MCH-S1/AuE (b), and RGO@AuNR-TH-SA/Hg^{2+}/biotin-S2/MCH-S1/AuE (c); **d** DPV curves of the TH/AuE (a), TH/AuNR/AuE (b), TH/RGO/AuE (c), and TH/RGO@AuNR/AuE (d)

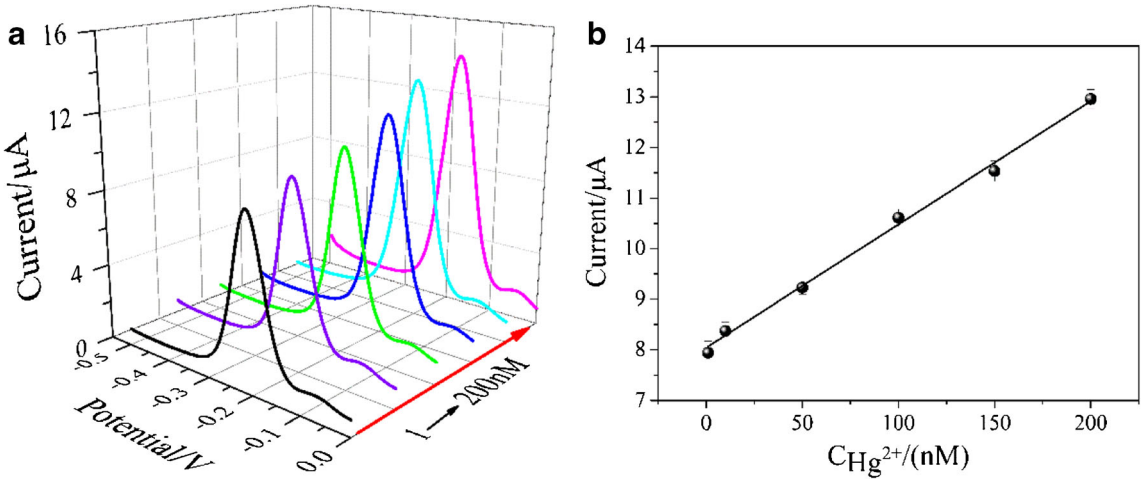

Fig. 4 **a** DPV responses of biosensor with different Hg^{2+} concentrations: 1, 10, 50, 100, 150, 200 nM in 50 mM Tris-HCl (pH 7.4) buffer. **b** Calibration plot of the biosensor toword different concentrations of Hg^{2+}. The data points came from the oxidation peak current value at working voltage −0.208 V (vs. Ag/AgCl)

shown in Fig. 4a, the DPV responses is linearly proportional to the Hg^{2+} concentration in the range of 1 nM–200 nM. As the Hg^{2+} concentration increased, the oxidation peak responses gradually increased. Figure 4b shows that the oxidation peak current value of TH vs Hg^{2+} concentration showed linearity in the range of 1 nM to 200 nM. The linear equation was I = 8.0441 + 0.02437c (nM) with a correlation coefficient of 0.995. The detection limit was calculated to be 0.24 nM (3 times the standard deviation of the blank) [19, 20]. This is lower than some other previous reports and can be ascribed to the performance of RGO@AuNR-TH-SA (Table 1). However, it took some more time for detection based on the DNA-based Hg^{2+} sensor, and there is still something for improvement.

Selectivity, reproducibility, repeatability and stability of the assay

100 nM of Hg^{2+}, 100 μM of other ions (Fe^{3+}, Cd^{2+}, Mg^{2+}, Co^{2+}, K^{+}, Pb^{2+}, Ag^{+}, Fe^{2+}, Mn^{2+}, Ca^{2+}, Cu^{2+} and Zn^{2+}), mixture of the afore-mentioned metal ions and blank sample are studied. As shown in Fig. 5, the biosensor exhibits high response to Hg^{2+} and mixture (including Hg^{2+}), but slight signal change to Cu^{2+}, Zn^{2+}, Mn^{2+} and Ca^{2+} or negligible signal change to other ions, indicating that the biosensor has excellent selectivity ($n = 5$). In addition, the reproducibility of the biosensor is studied by using six electrodes to detect Hg^{2+}, and the relative standard deviation (RSD) is found to be 5.41%, suggesting that the sensor has receivable reproducibility. The repeatability of the biosensor is estimated by six reduplicative measurements of an electrode, and the RSD is found to be 4.0%. After the electrode was stored at 4 °C for two weeks, the loss of current signal was about 7%, revealing the acceptable stability of the sensor.

Real sample analysis

The applicability of the biosensor is assessed by measuring the concentration of Hg^{2+} in tap water and waste water. The recovery experiment is researched by adding

Table 1 Analytical performance of various methods for Hg^{2+} detection

Detection method	Amplication strategy	Detection time	Liner range (nM)	Detection limit (nM)	Ref.
Fluorescence	Au NCs	1.5 h	37.5–3750	8.6	[21]
Fluorescence sensor	cysteamine-capped QDs	8	5–200	1	[22]
Fluorescence	Exonuclease III	2.5 h	0.05–10	0.031	[23]
Colorimetric sensor	Ag@GO	1 min	1×10^4–2×10^5	338	[24]
Colorimetric aptamer sensor	AuNPs	10 min	1–1×10^5	0.6	[25]
SPR sensor	SSG-rGO-Ag NSs	2 min	1×10^7–1×10^8	3.6	[26]
Electrochemical aptamer sensor	Fe_3O_4-SA	1 h	1–200	0.33	[27]
Electrochemical sensor	enzymatic BFC	25 min	1–100	1	[28]
Electrochemical DNA sensor	Exonuclease III	3 h	1–500	0.38	[29]
Electrochemical DNA sensor	GR@AuNRs-TH-SA	3 h	1–200	0.24	this work

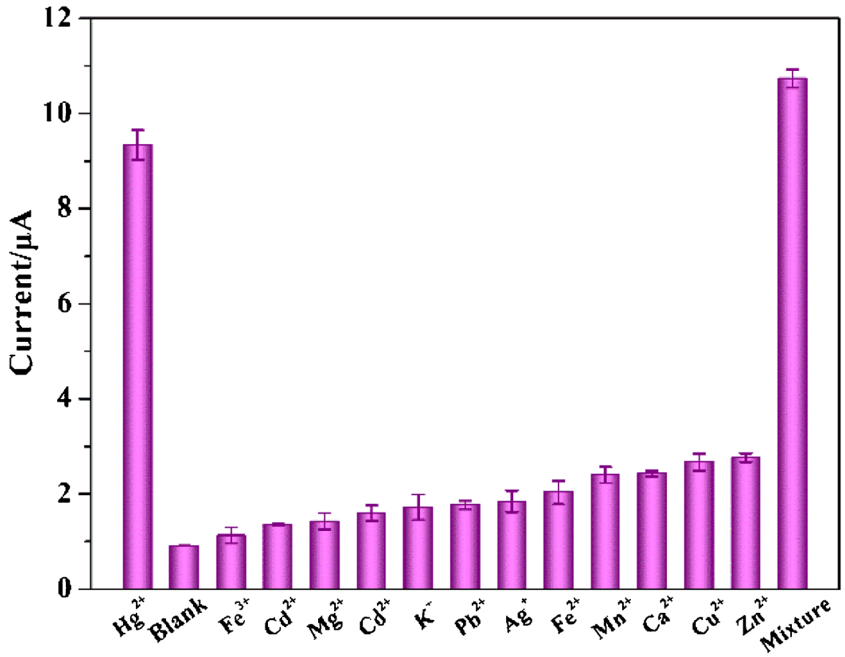

Fig. 5 Selectivity of the Hg^{2+} assay

three disparate concentrations of Hg^{2+} solution to the tap water and waste water samples. As shown in Table 2, the recoveries are between 96.71% and 104.02% with the RSD in the range of 1.46%–3.19% for the tap water sample. And the recoveries are between 91.23% and 105.43% with the RSD in the range of 1.50%–3.04% for the waste water sample. It indicates that the sensor has excellent accuracy for Hg^{2+} detection in real sample.

Conclusion

Based on T-Hg^{2+}-T structure and the RGO@AuNR-TH-SA, we constructed a novel Hg^{2+} electrochemical biosensor. The results indicate that RGO@AuNR is a good choice for strong adsorption to TH and SA, thus can improve the sensitivity of the biosensor. The biosensor also showed the favorable selectivity, reproducibility, repeatability and stability. Therefore, the method has a potential application prospect in the sensitive and selective detection of Hg^{2+}. However, it took some more time for detection based on the DNA-based Hg^{2+} sensor, and there are still something for improvement in the future.

Table 2 Detection of Hg^{2+} in water samples

Sample	Added (nM)	Found (nM)	RSD (%)	Recovery (%)
	1	1.04	1.46	104
Tap water	50	52.01	2.99	104.02
	100	96.71	3.19	96.71
	1	0.9123	2.48	91.23
Waste water	50	48.05	3.04	96.09
	100	105.43	1.50	105.43

Acknowledgments This study was funded by the Natural Science Foundation of Henan Province (182300410188), the Fundamental Research Funds for the Henan Provincial Colleges and Universities in Henan University of Technology (2016RCJH04), and Key Scientific and Technological Project of Henan Province (192102310255).

Compliance with ethical standards The author(s) declare that they have no competing interests.

References

1. Zhang RX, Deng L, Zhu PJ, Xu SX, Huang CP, Zeng Y, Ni SJ, Zhang XF (2017) Bienzyme-based visual and spectrophotometric aptamer assay for quantitation of nanomolar levels of mercury (II). Microchim Acta 184:541–546
2. Chen P, Wu P, Zhang YX, Chen JB, Jiang XM, Zheng CB, Hou XD (2016) Strand displacement-induced enzyme-free amplification for label-free and separation-free ultrasensitive atomic fluorescence spectrometric detection of nucleic acids and proteins. Anal Chem 88(24):12386
3. Denmark IS, Begu E, Arslan Z, Han FXX, Seiter-Moser JM, Pierce EM (2018) Removal of inorganic mercury by selective extraction and coprecipitation for determination of methylmercury in mercury-contaminated soils by chemical vapor generation inductively coupled plasma mass spectrometry (CVG-ICP-MS). Anal Chim Acta 1041:68–77
4. Wu Y, Jiang TT, Wu ZY, Yu RQ (2018) Novel ratiometric surface-enhanced raman spectroscopy aptasensor for sensitive and reproducible sensing of Hg^{2+}. Biosens Bioelectron 99:646–652

5. Gao F, Zhang TS, Chu YR, Wang QX, Song J, Qiu WW, Lin ZY (2018) Ultrasensitive impedimetric mercury(II) sensor based on thymine-Hg (II)-thymine interaction and subsequent disintegration of multiple sandwich-structured DNA chains. Microchim Acta 185: 555
6. Ono A, Togashi H (2004) High selective oligonucleotide-based sensor for mercury (II) in aqueous solutions. Angew Chem Int Ed 116(33):4400–4402
7. Wang H, Zhang YH, Ma HM, Ren X, Wang YG, Zhang Y, Wei Q (2016) Electrochemical DNA probe for Hg^{2+} detection based on a triple-helix DNA and multistage signal amplification strategy. Biosens Bioelectron 86:907–912
8. Luo JY, Jiang DF, Liu T, Peng JM, Chu ZY, Jin WQ (2018) High-performance electrochemical mercury aptasensor based on synergistic amplification of Pt nanotube arrays and Fe_3O_4/rGO nanoprobes. Biosens Bioelectron 104:1–7
9. Zuo YX, Xu JK, Zhu XF, Duan XM, Lu LM, Yu YF (2019) Graphene-derived nanomaterials as recognition elements for electrochemical determination of heavy metal ions: a review. Microchim Acta 186:171
10. Lu MH, Xiao R, Zhang XN, Niu JH, Zhang XT, Wang YM (2016) Novel electrochemical sensing platform for quantitative monitoring of hg(II) on DNA-assembled graphene oxide with target recycling. Biosens Bioelectron 85:267–271
11. Xu XL, Wei M, Liu YJ, Liu X, Wei W, Zhang YJ, Liu SQ (2017) A simple, fast, label-free colorimetric method for detection of telomerase activity in urine by using hemin-graphene conjugates. Biosens Bioelectron 87:600–606
12. Cao C, Zhai WT, Lu DD, Zhang HB, Zheng WG (2011) A facile method to prepare stable noncovalent functionalized graphene solution by using thionine. Mater Res Bull 46(4):583–587
13. Liu Y, Lv BJ, Liu AR, Liang GY, Yin LH, Pu YP, Wei W, Gou SH, Liu SQ (2018) Multicolor sensor for organophosphorus pesticides determination based on the bi-enzyme catalytic etching of gold nanorods. Sens Actuat B 265:675–681
14. Cao JT, Yang JJ, Zhao LZ, Wang YL, Wang H, Liu YM, Ma SH (2018) Graphene oxide@gold nanorods-based multiple-assisted electrochemiluminescence signal amplification strategy for sensitive detection of prostate specific antigen. Biosens Bioelectron 99: 92–98
15. Wei M, Zhang WY (2018) Ultrasensitive aptasensor with DNA tetrahedral nanostructure for Ochratoxin a detection based on hemin/G-quadruplex catalyzed polyaniline deposition. Sens Actuat B 276:1–7
16. Fathalipour S, Ataei B, Janati F (2019) Aqueous suspension of biocompatible reduced graphene oxide-au NPs composite as an effective recyclable catalyst in a Betti reaction. Mater Sci Eng C 97:356–366
17. Zhang PP, Huang Y, Lu X, Zhang SY, Li JF, Wei G, Su ZQ (2014) One-step synthesis of large-scale graphene film doped with gold nanoparticles at liquid-air Interface for electrochemistry and Raman detection applications. Langmuir 30:8980–8989
18. Li C, Zhao JY, Yan XY, Gu Y, Liu WL, Tang L, Zheng B, Li YR, Chen RX, Zhang ZQ (2015) Tremella-like grapheme-au composites used for amperometric determination of dopamine. Analyst 140(6):1913–1920
19. Qi YY, Xiu FR, Yu GD, Huang LL, Li BX (2017) Simple and rapid chemiluminescence aptasensor for Hg^{2+} in contaminated samples: a new signal amplification mechanism. Biosens Bioelectron 87:439–446
20. Li JS, Wang H, Guo ZK, Wang YG, Ma HM, Ren X, Du B, Wei Q (2017) A "turn-off" fluorescent biosensor for the detection of mercury (II) based on graphite carbon nitride. Talanta 162:46–51
21. Xu SH, Li XL, Mao YN, Gao T, Feng XY, Luo XL (2016) Novel dual ligand co-functionalized fluorescent gold nanoclusters as a versatile probe for sensitive analysis of Hg^{2+}, and oxytetracycline. Anal Bioanal Chem 408(11):2955–2962
22. Chen B, Ma J, Yang T, Chen L, Gao PF, Huang CZ (2017) A portable RGB sensing gadget for sensitive detection of Hg^{2+} using cysteamine-capped QDs as fluorescence probe. Biosens Bioelectron 98:36–40
23. Yu LL, Xu H, Chen H, Zhang SX, Jiang TT, Bai LJ, Wang WX, Gao SM, Jin J (2019) Label-free DNA Y junction for detection of Hg^{2+} using exonuclease III or graphene oxide-assisted background reduction. Microchem J 145:1086–1093
24. Kamali KZ, Pandikumar A, Jayabal S, Ramaraj R, Lim HN, Ong BH, Bien CSD, Kee YY, Huang NM (2016) Amalgamation based optical and colorimetric sensing of mercury(II) ions with silver@graphene oxide nanocomposite materials. Microchim Acta 183:369–377
25. Li L, Li BX, Qi YY, Jin Y (2009) Label-free aptamer-based colorimetric detection of mercury ions in aqueous media using unmodified gold nanoparticles as colorimetric probe. Anal Bioanal Chem 393(8):2051–2057
26. Manivannan S, Kang DK, Kim K (2018) Silicate sol-gel functionalized rGO-ag sensor-probe for spectral detection of Hg(II) ions. Mater Res Bull 106:144–151
27. Wu D, Wang YG, Zhang Y, Ma HM, Pang XH, Hu LH, Du B, Wei Q (2016) Facile fabrication of an electrochemical aptasensor based on magnetic electrode by using streptavidin modified magnetic beads for sensitive and specific detection of Hg^{2+}. Biosens Bioelectron 82:9–13
28. Wen D, Deng L, Guo SJ, Dong SJ (2011) Self-powered sensor for trace Hg^{2+} detection. Anal Chem 83(10):3968–3972
29. Fu CL, Yu H, Su LS, Liu C, Song YL, Wang SY, Lin ZY, Chen F (2018) Homogeneous electrochemical sensor for Hg^{2+} determination in environment water based on T-Hg^{2+}-T structure and exonuclease III-assisted recycling amplification. Analyst 143:2122–2127